Intermetallics 54 (2014) 110–119

Contents lists available at ScienceDirect

Intermetallics

journal homepage: www.elsevier.com/locate/intermet

First-principles studies on structural, mechanical, thermodynamic and electronic properties of Ni–Zr intermetallic compounds

Jinglian Du [a], Bin Wen [a, *], Roderick Melnik [b], Yoshiyuki Kawazoe [c, d]

[a] State Key Laboratory of Metastable Materials Science and Technology, Yanshan University, Qinhuangdao 066004, China
[b] M²NeT Lab, Wilfrid Laurier University, Waterloo, 75 University Ave. West, Ontario N2L 3C5, Canada
[c] New Industry Creation Hatchery Center, Tohoku University, 6-6-4 Aramaki-aza-Aoba, Aoba-ku, Sendai 980-8579, Japan
[d] Institute of Thermophysics, Siberian Branch of the Russian Academy of Sciences, 1, Lavyrentyev Avenue, Novosibirsk 630090, Russia

ARTICLE INFO

Article history:
Received 11 April 2014
Received in revised form
27 May 2014
Accepted 28 May 2014
Available online 18 June 2014

Keywords:
A. Intermetallics
B. Elastic properties
E. Ab-initio calculations
E. Phase stability, prediction
E. Physical properties

ABSTRACT

The structural, mechanical, thermodynamic and electronic properties of binary Ni–Zr intermetallic compounds have been investigated by performing first-principles calculations. The results indicated that the structural parameters of these Ni–Zr intermetallic compounds agree well with the available experimental and other theoretical values. With increasing of Zr-content, the mass density and bulk modulus of these Ni–Zr intermetallic compounds decrease. Besides, Ni_5Zr is the most stiffness phase and $NiZr_2$ is the most ductile phase among these binary Ni–Zr intermetallic compounds. The structural stability of these Ni–Zr alloys ascends with Zr-content increasing. Furthermore, all the binary Ni–Zr intermetallic compounds considered in this work are conductive phases, and they are thermodynamically stable.

1. Introduction

As one of the promising candidates for structural as well as functional materials, Ni–Zr binary alloys have been applied extensively due to their various superior properties, such as unique catalytic characteristics, specific hydrogen sorption properties, ultra-high fracture strength with good toughness, fine corrosion resistance and relatively low-cost [1–7]. Besides, the Ni–Zr binary alloy system is well known as a typical compound forming system [8–11]; meanwhile, it is also a system in which amorphous alloys can be formed over wide composition ranges [12–16]. Therefore, the alloy phases in Ni–Zr binary system including Ni–Zr intermetallic compounds and Ni–Zr amorphous alloys have drawn considerable attention.

To the binary Ni–Zr alloy system, researchers have found that there are close relationships between the crystalline phases and amorphous phases in the compositional as well as structural characteristics [17–31]. For example, the amorphous Ni–Zr alloys with good glass forming ability are usually located at or near the eutectic points in the Ni–Zr binary phase diagram [12,25,31]; there are 'crystal-like' short range structures in the Ni–Zr amorphous alloys, which further implies that a correlation exists in the short range order between Ni–Zr amorphous phases and the crystalline phases to which they transform [17,18,26,29]; the Ni–Zr intermetallic compounds can be amorphized through the mechanical alloying method [19–21]. In this context, it is proposed to be a feasible method to investigate the amorphous Ni–Zr alloys based on the corresponding Ni–Zr intermetallic compounds.

In the past decades, significant progresses have been made on the studies of crystalline phases and amorphous phases in the binary Ni–Zr alloy system [32–41]. Nevertheless, the existing researches of Ni–Zr alloys are mainly focused on the glass forming composition ranges, amorphization and crystallization characteristics. As for the intermetallic compounds (i.e. Ni_5Zr, Ni_7Zr_2, $Ni_{23}Zr_6$, Ni_3Zr, $Ni_{21}Zr_8$, Ni_2Zr, $Ni_{10}Zr_7$, $Ni_{11}Zr_9$, NiZr and $NiZr_2$) existing in binary Ni–Zr alloy system [42,43], only several phases have been studied. For example, Henaff et al. explored the crystallization behavior of binary Ni–Zr alloy system in 1984, and experimentally obtained the enthalpies of formation for Ni_5Zr, Ni_7Zr_2, $Ni_{10}Zr_7$, NiZr and $NiZr_2$ [32]. Lee et al. investigated the formation of Ni–Zr amorphous alloys by mechanical alloying of the mixtures of $Ni_{11}Zr_9$ and $NiZr_2$ intermetallic compounds in 1987 [20]. Ohsaka et al. investigated the Gibbs free-energy difference between the glass and crystalline phases of Ni–Zr alloys in 1993 [38]. Joubert et al. studied the hydrogen absorption properties of $Ni_{11}Zr_9$, $Ni_{10}Zr_7$,

* Corresponding author. Tel.: +86 335 8568761.
E-mail address: wenbin@ysu.edu.cn (B. Wen).

http://dx.doi.org/10.1016/j.intermet.2014.05.021
0966-9795/

$Ni_{21}Zr_8$ and Ni_7Zr_2 in 1995 [40]. Jaksic et al. investigated the Ni–Zr intermetallic electro-catalysis for hydrogen electrode reactions in 2000 [39]. In the same year, Spriano et al. performed the surface and electrochemical characterization of Ni–Zr intermetallic compounds [23]. Abe et al. carried out a thermodynamic assessment of the binary Ni–Zr alloy system in 2005 [11]. Liu et al. studied the local atomic structures of Ni–Zr metallic glasses and the correlations with their intermetallic compounds counterparts in 2009 [26]. Mihailov et al. explored the effect of microstructure on the electro-catalytic activity for hydrogen evolution of amorphous and nanocrystalline Ni–Zr alloys in 2012, and demonstrated that the nanocrystal presents better catalytic performance than the entirely amorphous alloys with the same composition in Ni–Zr alloy system [41]. Huang et al. investigated the structural and thermal properties of binary Ni–Zr alloys by melt spinning and copper mold casting methods in 2013 [1]. As mentioned above, we can see that the previous studies for binary Ni–Zr intermetallic compounds are concerned mostly about their electro-catalysis features and hydrogen storage properties. So far, to the best of our knowledge, there are no reported results for other material properties of the binary Ni–Zr intermetallic compounds. From this viewpoint, further studies along this direction are still in demand. In the following sections, the component-related structural, mechanical, thermodynamic and electronic properties of binary Ni–Zr intermetallic compounds have been studied in detail by performing first-principles calculations.

2. Computational methods

In this work, the crystallographic data of binary Ni–Zr intermetallic compounds are taken from Ref. [44], as shown in Table 1. The first-principles calculations have been performed within the framework of electronic density functional theory (DFT), as implemented in the Vienne Ab initio Simulation Package (VASP) [45]. The exchange and correlation interaction was described by the generalized gradient approximation (GGA) with the Perdew–Wang (PW91) parameterization [46]. The interactions between ions and valence electrons were modeled by the projector-augmented wave (PAW) method [47]. The pseudopotentials employed in this work explicitly treat ten valence electrons for nickel (Ni $3d^84s^2$) and four for zirconium (Zr $4d^25s^2$). A plain wave cutoff energy for 330 eV has been used. Brillouin zone integrations were modeled by using a Monkhorst–Pack k-point mesh [48], and the k-point mesh of each cell has been sampled by $4 \times 4 \times 4$, $2 \times 2 \times 2$, $4 \times 4 \times 4$, $5 \times 5 \times 6$, $4 \times 3 \times 3$, $4 \times 4 \times 4$, $3 \times 3 \times 2$, $2 \times 3 \times 3$, $3 \times 3 \times 4$, $8 \times 3 \times 6$ and $4 \times 4 \times 5$ grids for Ni_5Zr, $Ni_{23}Zr_6$, Ni_7Zr_2, Ni_3Zr, $Ni_{21}Zr_8$, Ni_2Zr, Aba2-$Ni_{10}Zr_7$, Pbca-$Ni_{10}Zr_7$, $Ni_{11}Zr_9$, NiZr and $NiZr_2$, respectively. The total energy was converged numerically to 5×10^{-7} eV/atom with respect to electronic, ionic and unit cell degrees of freedom.

To verify computational accuracy, benchmark calculations have been performed for the Ni_3Zr intermetallic compound. The lattice parameters ($a = 0.5324$ nm, $c = 0.4320$ nm), after optimization for the bulk Ni_3Zr phase, agree well with the available experimental ($a = 0.5309$ nm, $c = 0.4303$ nm) [44] and previously reported theoretical ($a = 0.5299$ nm, $c = 0.4382$ nm) values [27], which confirms that the computational scheme used in this work is reliable.

3. Results and discussion

3.1. The structural parameters

The lattice parameters and atomic internal coordinates of these binary Ni–Zr intermetallic compounds have been optimized by performing first-principles calculations. Table 1 presents the optimized lattice parameters and the corresponding mass densities, together with the available experimental and other theoretical values known from the literatures. As shown in Table 1, the calculated results are consistent well with previously reported experimental and other theoretical values [27,44]. Furthermore, the correlations between the mass density and Zr-content for these Ni–Zr intermetallic compounds are plotted in Fig. 1, from which we can see that the mass densities of these binary Ni–Zr intermetallic compounds decrease almost monotonously with the increase of Zr-

Table 1
Theoretical and experimental crystallographic data and mass density for the binary Ni–Zr system intermetallic compounds.

Phase	Space group	Prototype	Pearson symbol	Unit cell lattice parameters (nm)			Mass density (kg/m^3)	Reference
Ni	$Fm\bar{3}m$	Cu	cF4	$a = 0.3516$			8975.4	This work
				$a = 0.3523$				[44]
							8910.0	[54]
Ni_5Zr	$F\bar{4}3m$	$AuBe_5$	cF24	$a = 0.6713$			8449.2	This work
				$a = 0.6708$				[44]
$Ni_{23}Zr_6$	$Fm\bar{3}m$	$Mn_{23}Th_6$	cF116	$a = 1.1493$			8302.3	This work
				$a = 1.1353$				[44]
Ni_7Zr_2	C2/m	Ni_7Zr_2	mC36	$a = 0.4704$	$b = 0.8239$	$c = 0.6532$	8343.6	This work
				$a = 0.4699$	$b = 0.8235$	$c = 1.2193$		[44]
Ni_3Zr	$P6_3/mmc$	Ni_3Sn	hP8	$a = 0.5324$		$c = 0.4320$	8373.3	This work
				$a = 0.5309$		$c = 0.4303$		[44]
$Ni_{21}Zr_8$	$P\bar{1}$	$Ni_{21}Hf_8$	aP29	$a = 0.6469$	$b = 0.8095$	$c = 0.8586$	7491.7	This work
				$a = 0.6472$	$b = 0.8065$	$c = 0.8588$		[44]
Ni_2Zr	$Fd\bar{3}m$	Cu_2Mg	cF24	$a = 0.6978$			8156.9	This work
				$a = 0.6916$				[44]
Aba2-$Ni_{10}Zr_7$	Aba2	$Ni_{10}Zr_7$	oC68	$a = 0.9194$	$b = 0.9195$	$c = 1.2441$	7739.5	This work
				$a = 0.9211$	$b = 0.9157$	$c = 1.2387$	7780.0	[44]
Pbca-$Ni_{10}Zr_7$	Pbca	$Ni_{10}Zr_7$	oP68	$a = 1.2446$	$b = 0.9191$	$c = 0.9200$	7735.8	This work
				$a = 1.2497$	$b = 0.9210$	$c = 0.9325$	7680.0	[44]
$Ni_{11}Zr_9$	I4/m	$Pt_{11}Zr_9$	tI40	$a = 1.0012$		$c = 0.6472$	7508.4	This work
				$a = 0.9881$		$c = 0.6611$		[44]
NiZr	Cmcm	BCr	oC8	$a = 0.3303$	$b = 1.0012$	$c = 0.4080$	7380.1	This work
				$a = 0.3268$	$b = 0.9937$	$c = 0.4102$	7473.0	[44]
$NiZr_2$	I4/mcm	Al_2Cu	tI12	$a = 0.6515$		$c = 0.5221$	7228.1	This work
				$a = 0.6488$		$c = 0.5265$		[44]
Zr	$P6_3/mmc$	Mg	hP2	$a = 0.3231$		$c = 0.5174$	6475.6	This work
				$a = 0.3232$		$c = 0.5148$	6487.0	[44]

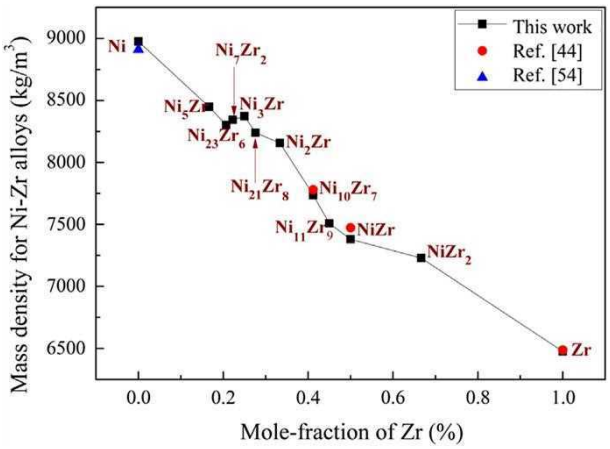

Fig. 1. Theoretical mass density compared to experimental values for the binary Ni–Zr system intermetallic compounds, the connecting lines are just a "guide for eye".

contents. This can be understood from the fact that the mass density of pure zirconium (6475.55 kg/m^3) is smaller than that of pure nickel (8975.36 kg/m^3). Subsequently, it is deduced that the correlations between the Zr-contents c (at. %) and mass density ρ (kg/m^3) of these Ni–Zr intermetallic compounds can be expressed as the following formula: $\rho = 8878.79\text{-}2556.89c$.

3.2. The mechanical properties

To investigate the phase stability and relevant material properties of these binary Ni–Zr intermetallic compounds, first-principles calculations have been performed to obtain the single-crystal elastic constants of the related phases with their stable ground state structures. In this study, the single-crystal elastic constants were obtained by computing the total energy density as a function of suitable strains [49,50]. Depending on the crystal systems and various imposed deformations, the quadratic coefficient of the total energy density versus strain corresponds to either a specific elastic constant or a linear combination of several elastic constants [51,52]. In this work, the total energies of the relevant phases have been calculated by imposing appropriate strains up to ±1.25% at 0.25% interval.

Accordingly, the single-crystal elastic constants of these binary Ni–Zr intermetallic compounds as well as pure nickel and zirconium have been calculated. The corresponding values are summarized in Table 2, along with the available experimental and other theoretical values known from the literature. The results indicated that for Ni_3Zr, NiZr, pure nickel and zirconium, our calculated single-crystal elastic constants are in good agreement with the existing experimental and theoretical values [27,53–57]. Nevertheless, as far as we known, there are no reported data of single-crystal elastic constants for other binary Ni–Zr intermetallic compounds in the literature. In this regard, our calculated results of single-crystal elastic constants for Ni_5Zr, $Ni_{23}Zr_6$, Ni_7Zr_2, $Ni_{21}Zr_8$, Ni_2Zr, Aba2-$Ni_{10}Zr_7$, Pbca-$Ni_{10}Zr_7$, $Ni_{11}Zr_9$ and $NiZr_2$ intermetallic compounds will provide new readily available information for the comparison with future experimental measurements as well as theoretical investigations.

3.2.1. The mechanical stability

It is well known that the mechanical stability is one of the important theoretical research fields on the phase stability of materials. In the light of the mechanical stability evaluation criteria, the information on the mechanical stability of an alloy phase can be acquired from the knowledge of its corresponding single-crystal elastic constants [58]. As for the binary Ni–Zr intermetallic compounds considered in this work, Ni_5Zr, Ni_2Zr and $Ni_{23}Zr_6$ belong to the cubic crystal system; $Ni_{11}Zr_9$ and $NiZr_2$ belong to the tetragonal crystal system; Ni_3Zr belongs to the hexagonal crystal system; Aba2-$Ni_{10}Zr_7$, Pbca-$Ni_{10}Zr_7$ and NiZr belong to the orthorhombic crystal system; and Ni_7Zr_2 belongs to the monoclinic crystal system.

Table 2
Calculated single-crystal elastic constants for the binary Ni–Zr system intermetallic compounds, compared to experimental and other theoretical values known from the literature.

Phase	Single-crystal elastic constants (GPa)							Reference
Ni	$C_{11} = 240.89$	$C_{12} = 176.98$	$C_{44} = 113.34$					This work
	$C_{11} = 261.2$	$C_{12} = 150.8$	$C_{44} = 131.7$					[53]
	$C_{11} = 248.1$	$C_{12} = 154.9$	$C_{44} = 124.2$					[54]
Ni_5Zr	$C_{11} = 291.87$	$C_{12} = 130.13$	$C_{44} = 97.10$					This work
$Ni_{23}Zr_6$	$C_{11} = 270.08$	$C_{12} = 136.30$	$C_{44} = 95.73$					This work
Ni_7Zr_2	$C_{11} = 178.86$	$C_{12} = 0.49$	$C_{13} = -4.27$	$C_{22} = 136.23$	$C_{23} = -4.42$	$C_{33} = 204.90$	$C_{15} = 0.59$	This work
	$C_{25} = 0.60$	$C_{35} = 0.63$	$C_{44} = 72.70$	$C_{46} = -11.36$	$C_{55} = 51.61$	$C_{66} = 72.58$		
Ni_3Zr	$C_{11} = 292.18$	$C_{12} = 118.42$	$C_{13} = 106.71$	$C_{33} = 327.17$	$C_{44} = 59.93$			This work
	$C_{11} = 285.1$	$C_{12} = 125.8$	$C_{13} = 113.3$	$C_{33} = 307.1$	$C_{44} = 66.6$			[27]
	$C_{11} = 278.4$	$C_{12} = 113.5$	$C_{13} = 112.5$	$C_{33} = 292.9$	$C_{44} = 49.6$			[27]
$Ni_{21}Zr_8$	$C_{11} = 205.28$	$C_{12} = 85.68$	$C_{13} = 70.70$	$C_{14} = -0.96$	$C_{15} = 4.02$	$C_{16} = -11.95$	$C_{22} = 181.58$	This work
	$C_{23} = 79.05$	$C_{24} = 5.31$	$C_{25} = -8.44$	$C_{26} = 5.69$	$C_{33} = 197.81$	$C_{34} = -9.12$	$C_{35} = 19.29$	
	$C_{36} = 15.33$	$C_{44} = 39.48$	$C_{45} = 16.19$	$C_{46} = -11.68$	$C_{55} = 58.92$	$C_{56} = 16.19$	$C_{66} = 43.37$	
Ni_2Zr	$C_{11} = 243.13$	$C_{12} = 127.34$	$C_{44} = 99.35$					This work
Aba2-$Ni_{10}Zr_7$	$C_{11} = 208.74$	$C_{12} = 120.01$	$C_{13} = 121.97$	$C_{22} = 211.40$	$C_{23} = 119.78$	$C_{33} = 208.17$	$C_{44} = 56.05$	This work
	$C_{55} = 55.31$	$C_{66} = 52.72$						
Pbca-$Ni_{10}Zr_7$	$C_{11} = 208.52$	$C_{12} = 119.80$	$C_{13} = 121.65$	$C_{22} = 211.28$	$C_{23} = 119.91$	$C_{33} = 208.49$	$C_{44} = 52.39$	This work
	$C_{55} = 55.28$	$C_{66} = 55.96$						
$Ni_{11}Zr_9$	$C_{11} = 202.93$	$C_{12} = 120.95$	$C_{13} = 108.62$	$C_{33} = 202.63$	$C_{44} = 42.19$	$C_{66} = 51.70$		This work
NiZr	$C_{11} = 172.93$	$C_{12} = 111.88$	$C_{13} = 118.45$	$C_{22} = 201.90$	$C_{23} = 115.66$	$C_{33} = 211.85$	$C_{44} = 79.76$	This work
	$C_{55} = 63.10$	$C_{66} = 15.67$						
	$C_{11} = 176$	$C_{12} = 104$	$C_{13} = 126$	$C_{22} = 215$	$C_{23} = 119$	$C_{33} = 185$	$C_{44} = 79$	[57]
	$C_{55} = 64$	$C_{66} = 14$						
$NiZr_2$	$C_{11} = 160.81$	$C_{12} = 113.41$	$C_{13} = 92.43$	$C_{33} = 170.00$	$C_{44} = 27.44$	$C_{66} = 21.17$		This work
Zr	$C_{11} = 159.83$	$C_{12} = 53.97$	$C_{13} = 67.28$	$C_{33} = 180.61$	$C_{44} = 18.94$			This work
	$C_{11} = 137.77$	$C_{12} = 71.67$	$C_{13} = 70.99$	$C_{33} = 159.98$	$C_{44} = 23.30$			[56]
	$C_{11} = 156.4$	$C_{12} = 65.4$	$C_{13} = 75.8$	$C_{33} = 182.0$	$C_{44} = 24.8$			[55]

The restrictions of mechanical stability for cubic crystal system structures [58] are given by the following formulas (1):

$$C_{11} > 0, C_{44} > 0, C_{11} > |C_{12}|, C_{11} + 2C_{12} > 0 \quad (1)$$

From the results listed in Table 2, we can see that the elastic constants of the cubic crystal system structures Ni_5Zr, Ni_2Zr and $Ni_{23}Zr_6$ coincide with the above mechanical stability requirements, signifying that they are mechanically stable phases.

The requirements of mechanical stability criteria for tetragonal crystal system structures [58] are given by the following formulas (2):

$$C_{11} > 0, C_{33} > 0, C_{44} > 0, C_{66} > 0, C_{11} - C_{12} > 0, C_{11} + C_{33} - 2C_{13} > 0, 2(C_{11} + C_{12}) + C_{33} + 4C_{13} > 0 \quad (2)$$

As shown in Table 2, all the values of elastic constants for tetragonal crystal system structures $Ni_{11}Zr_9$ and $NiZr_2$ satisfy the mechanical stability restrictions of formulas (2), confirming that $Ni_{11}Zr_9$ and $NiZr_2$ are mechanically stable.

For hexagonal crystal system structures, the mechanical stability restrictions [58] are given by the following formulas (3):

$$C_{44} > 0, C_{11} > |C_{12}|, (C_{11} + 2C_{12})C_{33} > 2C_{13}^2 \quad (3)$$

As can be seen, the single-crystal elastic constants in Table 2 for the hexagonal crystal system structure Ni_3Zr satisfy completely the above mechanical stability criteria, confirming that Ni_3Zr is a mechanically stable phase.

In terms of orthorhombic crystal system structures, the mechanical stability requirements [58] are given by the following formulas (4):

$$C_{11} > 0, C_{22} > 0, C_{33} > 0, C_{44} > 0, C_{55} > 0, C_{66} > 0, C_{11} + C_{22} + C_{33} + 2(C_{12} + C_{13} + C_{23}) > 0, C_{11} + C_{22} - 2C_{12} > 0, C_{11} + C_{33} - 2C_{13} > 0, C_{22} + C_{33} - 2C_{23} > 0 \quad (4)$$

As follows from the single-crystal elastic constants shown in Table 2, all the orthorhombic crystal system structures of intermetallic compounds in binary Ni–Zr alloy system meet the mechanical stability criteria in formulas (4), demonstrating that Aba2-$Ni_{10}Zr_7$, Pbca-$Ni_{10}Zr_7$ and NiZr are mechanically stable.

The mechanical stability criteria for monoclinic crystal system structures [58] are given by the following formulas (5):

$$C_{11} > 0, C_{22} > 0, C_{33} > 0, C_{44} > 0, C_{55} > 0, C_{66} > 0, [C_{11} + C_{22} + C_{33} + 2(C_{12} + C_{13} + C_{23})] > 0, (C_{33}C_{55} - C_{35}^2) > 0, (C_{44}C_{66} - C_{46}^2) > 0, (C_{22} + C_{33} - 2C_{23}) > 0, [C_{22}(C_{33}C_{55} - C_{35}^2) + 2C_{23}C_{25}C_{35} - C_{23}^2 C_{55} - C_{25}^2 C_{33}] > 0, 2[C_{15}C_{25}(C_{33}C_{12} - C_{13}C_{23}) + C_{15}C_{35}(C_{22}C_{13} - C_{12}C_{23}) + C_{25}C_{35}(C_{11}C_{23} - C_{12}C_{13})] - [C_{15}^2(C_{22}C_{33} - C_{23}^2) + C^2{}_{25}(C_{11}C_{33} - C_{13}^2) + C_{35}^2(C_{11}C_{22} - C_{12}^2)] + C_{55}(C_{11}C_{22}C_{33} - C_{11}C_{23}^2 - C_{22}C_{13}^2 - C_{33}C_{12}^2 + 2C_{12}C_{13}C_{23})\} > 0 \quad (5)$$

As is shown in Table 2, the elastic constants of monoclinic crystal system structure Ni_7Zr_2 satisfy these mechanical stability requirements, confirming that Ni_7Zr_2 is a mechanically stable phase.

Accordingly, we conclude that the Ni_5Zr, $Ni_{23}Zr_6$, Ni_7Zr_2, Ni_3Zr, Ni_2Zr, Aba2-$Ni_{10}Zr_7$, Pbca-$Ni_{10}Zr_7$, $Ni_{11}Zr_9$, NiZr and $NiZr_2$ intermetallic compounds are mechanically stable.

3.2.2. The elastic properties

On the basis of the obtained single-crystal elastic constants, the elastic moduli including bulk modulus (K), shear modulus (G) and Young's modulus (E), along with Poisson's ratio (u) for the corresponding polycrystalline materials have been deduced by using Voigt, Reuss and Hill (VRH) approximations [59,60], with a view to investigate the mechanical properties of the binary Ni–Zr intermetallic compounds. The obtained results are presented in Table 3, together with the available values known from the literatures. Then, the component-related variations of elastic modulus for these binary Ni–Zr intermetallic compounds have been explored further. In this work, it is noteworthy that the connecting lines of the specific Figures reflecting the changes of related parameters as Zr-contents are just a "guide for eye" and only used to denote the variation trend, since there are no precise functional relations between these parameters. The variation of bulk modulus with Zr-content (i.e. mole fraction of Zr) has been plotted in Fig. 2. It shows that in general, the bulk modulus of Ni–Zr intermetallic compounds decreases with the increase of Zr-content, but it does not following a strict linear correlation. Furthermore, researchers have found that a certain connection exists between the bulk modulus and mass density of materials [61,62], thus comparing Figs. 1 and 2, we can see that the variation trend of bulk modulus with Zr-content (at %) is analogous to that of the mass density for these Ni–Zr intermetallic compounds. Subsequently, the relationship between mass density and bulk modulus of these binary Ni–Zr intermetallic compounds is depicted in Fig. 3. As is shown, the bulk modulus increases with the increase of mass density for these binary Ni–Zr intermetallic compounds. This result further confirms the thesis that there exists a positive correlation between mass density and bulk modulus of materials [62,63]. Afterwards, the variations of shear modulus (G) and Young's modulus (E) with Zr-content (at %) are reflected in Fig. 4. As can be seen, among these binary Ni–Zr intermetallic compounds, Ni_5Zr possesses the largest shear modulus of 90.24 GPa and Young's modulus of 232.70 GPa, while $NiZr_2$ has the smallest shear modulus of 27.43 GPa and Young's modulus of 76.50 GPa. Indeed, the hardness of materials

Table 3
Polycrystalline shear modulus (G), bulk modulus (K), Young's modulus (E), Poisson's ratio (u) and G/K ratio for the binary Ni–Zr system intermetallic compounds, deduced from the single-crystal elastic constants via Voigt, Ruess and Hill (VRH) approximations.

Phase	G (GPa)	K (GPa)	E (GPa)	u	G/K	Reference
Ni_5Zr	90.24	184.04	232.70	0.2893	0.4903	This work
Ni_3Zr	77.99	174.93	203.71	0.3059	0.4458	This work
	76.87	175.77	201.27	0.3092	0.4373	[27]
	68.12	169.60	180.23	0.3229	0.4016	[27]
$Ni_{23}Zr_6$	82.92	180.89	215.78	0.3012	0.4584	This work
Ni_2Zr	80.00	165.94	206.77	0.2923	0.4821	This work
Aba2-$Ni_{10}Zr_7$	50.31	150.20	135.77	0.3493	0.3349	This work
Pbca-$Ni_{10}Zr_7$	50.26	150.11	135.63	0.3494	0.3348	This work
$Ni_{11}Zr_9$	45.03	142.70	122.24	0.3572	0.3156	This work
NiZr	41.32	141.35	112.96	0.3668	0.2923	This work
	39	141			0.2778	[57]
$NiZr_2$	27.43	120.84	76.50	0.3945	0.2270	This work
Ni	68.46	198.28	184.19	0.3452	0.3453	This work
Zr	34.79	97.06	93.24	0.3399	0.3585	This work

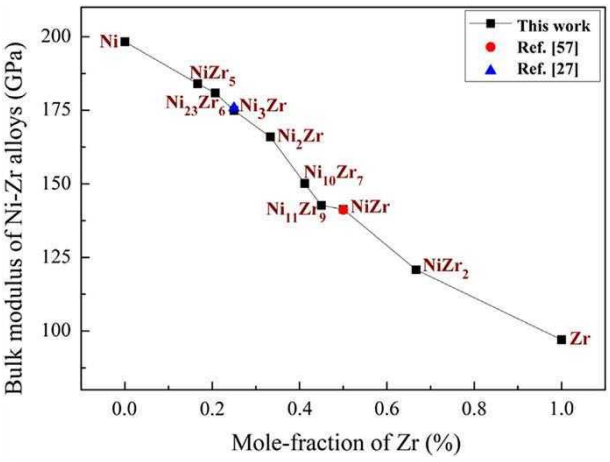

Fig. 2. Variation trend of bulk modulus versus Zr-content's for the binary Ni–Zr system intermetallic compounds, the connecting lines are just a "guide for eye".

can be estimated from their shear modulus and Young's modulus, even though the precise relations between these two parameters are still unclear to date [64]. We note also that a large elastic modulus often signifies a high hardness material [65]. Accordingly,

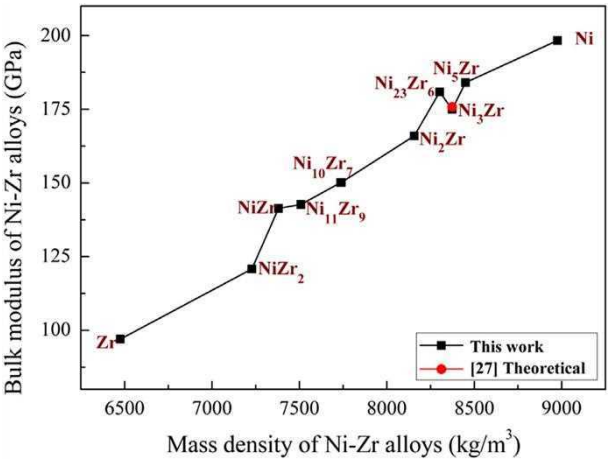

Fig. 3. Variation trend of bulk modulus versus mass density for the binary Ni–Zr system intermetallic compounds, the connecting lines are just a "guide for eye".

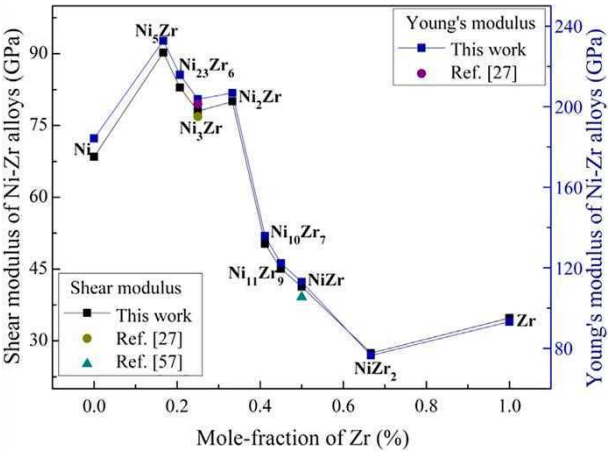

Fig. 4. Variation trend of shear modulus and Young's modulus versus Zr-content for the binary Ni–Zr system intermetallic compounds, the connecting lines are just a "guide for eye".

Ni_5Zr has the highest hardness and $NiZr_2$ has the lowest hardness among the Ni–Zr intermetallic compounds considered here.

To further explore the mechanical properties of these Ni–Zr intermetallic compounds, the ratio of shear modulus to bulk modulus (G/K), which can be used to predict the brittleness and toughness of materials [66], is calculated on the basis of the obtained elastic modulus. The corresponding results are summarized in Table 3. The critical value of the G/K ratio is 0.57, i.e. phases whose G/K value is larger than 0.57 are considered brittle, otherwise they are ductile [66]. This criterion has been demonstrated to be reliable for the intermetallic compounds in many alloy systems [67–70]. Usually, the lower ratio of G/K, the more ductile the materials would be. As shown in Table 3, the G/K ratio for the Ni_5Zr, Ni_3Zr, $Ni_{23}Zr_6$, Ni_2Zr, Aba2-$Ni_{10}Zr_7$, Pbca-$Ni_{10}Zr_7$, $Ni_{11}Zr_9$, NiZr and $NiZr_2$ are lower than the critical value of 0.57, signifying that they are ductile phases. Meanwhile, $NiZr_2$ is the most ductile phase among these binary Ni–Zr intermetallic compounds. Moreover, since Poisson's ratio can be used as another effective parameter to evaluate the ductility of materials [71], both the Poisson's ratio and G/K ratio versus the Zr-content have been plotted to further study the brittleness and toughness of these binary Ni–Zr intermetallic compounds, and the results are reflected in Fig. 5. As can be seen that the variations of G/K ratio and Poisson's ratio present the opposite trend with the increase of Zr-content, and they are in one-to-one correspondence. Subsequently, the correlations between G/K ratio and Poisson's ratio for the binary Ni–Zr intermetallic compounds are depicted in Fig. 6, from which we can see that these two ratios are exactly linearly dependent for these Ni–Zr intermetallic compounds. And this linear relation can be further expressed as: $u = -0.396G/K + 0.483$. In the meantime, these results further reveal the correlations between ratio of shear modulus to bulk modulus and Poisson's ratio for isotropic materials [72].

Besides, considering the close correlations between the amorphous alloy phases and their corresponding crystalline counterparts [73,74], our investigations on the elastic properties of these binary Ni–Zr intermetallic compounds will provide useful information for researchers to further study the related properties of NiZr-based complex metallic alloy phases.

3.3. The thermodynamic properties

The thermodynamic properties of a phase can be acquired from its heats of formation and cohesive energy [39], thus both the heats of formation and cohesive energies for these binary Ni–Zr

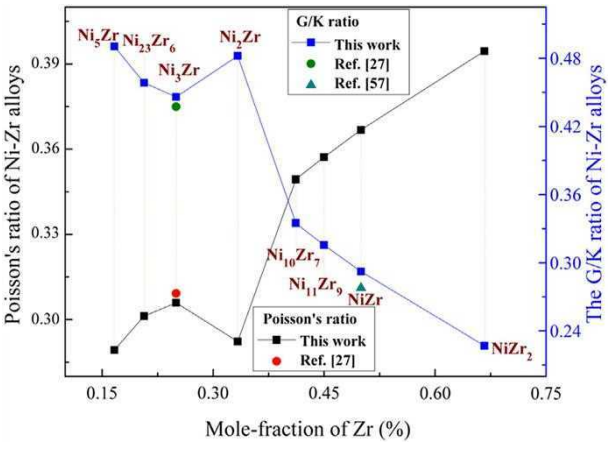

Fig. 5. Variation trend of shear modulus to bulk modulus's ratio (G/K) and Poisson's ratio (u) versus Zr-content for the binary Ni–Zr system intermetallic compounds, the connecting lines are just a "guide for eye".

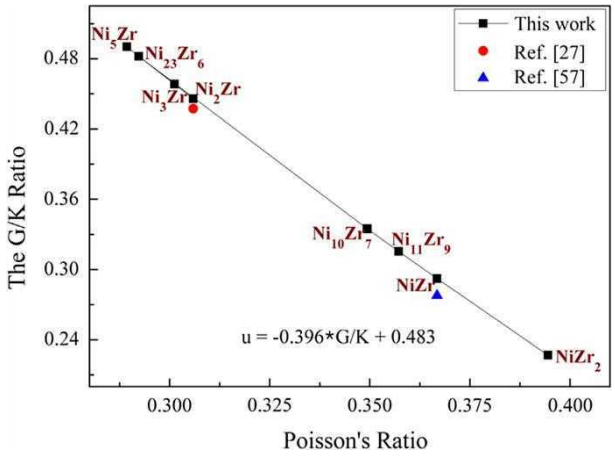

Fig. 6. Shear modulus to bulk modulus's ratio (G/K) versus Poisson's ratio (u) for the binary Ni–Zr system intermetallic compounds.

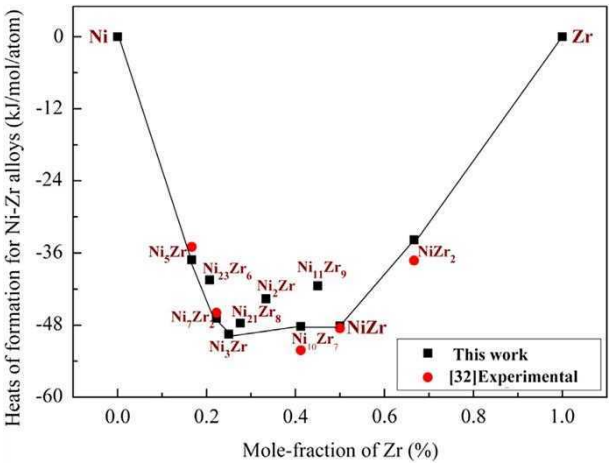

Fig. 7. Calculated heats of formation compared to experimental values for the binary Ni–Zr system intermetallic compounds.

intermetallic compounds have been computed and analyzed in the following part to understand their thermodynamic equilibrium characteristics.

3.3.1. Heats of formation

The ground state total energies of these binary Ni–Zr intermetallic compounds as well as pure nickel and zirconium have been calculated to obtain the heats of formation. In terms of a specific binary intermetallic compound Ni_aZr_b, the heats of formation is defined as the difference between the total energy of Ni_aZr_b and the linear combination of the pure nickel and pure zirconium stable state energies [56,70]. Correspondingly, the heats of formation for a certain Ni_aZr_b intermetallic compound can be obtained from the following formula (6):

$$E_{\text{form}}^{\text{Ni}_a\text{Zr}_b} = \left[E_{\text{total}}^{\text{Ni}_a\text{Zr}_b} - \left(aE_{\text{solid}}^{\text{Ni}} + bE_{\text{solid}}^{\text{Zr}}\right)\right] \Big/ (a+b) \tag{6}$$

In formula (6), $E_{\text{form}}^{\text{Ni}_a\text{Zr}_b}$ denotes the heats of formation for the Ni_aZr_b alloy phase, $E_{\text{total}}^{\text{Ni}_a\text{Zr}_b}$ is the total energy of the Ni_aZr_b primitive cell containing "a" Ni atoms and "b" Zr atoms with its stable ground state structure, $E_{\text{solid}}^{\text{Ni}}$ is the total energy of one Ni atom in face-centered cubic structure with its equilibrium lattice parameters, and $E_{\text{solid}}^{\text{Zr}}$ is the total energy of one Zr atom with the hexagonal close-packed structure in its corresponding equilibrium lattice parameters. Accordingly, the formation energies of these binary Ni–Zr intermetallic compounds considered here have been calculated. The results are summarized in Table 4, together with the available experimental values known from the literature [32]. Subsequently, the stoichiometry-dependent formation energies for these binary Ni–Zr intermetallic compounds have been further depicted in Fig. 7. It is noteworthy that we have taken the ground state convex hull defined by Ni_5Zr, Ni_7Zr_2, Ni_3Zr, $Ni_{10}Zr_7$, NiZr and $NiZr_2$ in this study, since the six intermetallic compounds are stable phases in the binary Ni–Zr alloy system at 0 K [32,43].

Table 4
The heats of formation for the binary Ni–Zr system intermetallic compounds, calculated in this work and known from the literature.

Phase	Heats of formation (kJ/mol atoms)	Reference
Ni_5Zr	−37.108	This work
	−34.98	[32]
$Ni_{23}Zr_6$	−40.465	This work
Ni_7Zr_2	−46.863	This work
	−45.94	[32]
Ni_3Zr	−49.485	This work
$Ni_{21}Zr_8$	−47.655	This work
Ni_2Zr	−43.616	This work
Aba2-$Ni_{10}Zr_7$	−48.216	This work
	−52.17	[32]
Pbca-$Ni_{10}Zr_7$	−48.218	This work
$Ni_{11}Zr_9$	−41.466	This work
NiZr	−48.137	This work
	−48.53	[32]
$NiZr_2$	−33.817	This work
	−37.24	[32]

According to the calculated heats of formation, the relative stability of these binary Ni–Zr intermetallic compounds has been analyzed. As shown in Fig. 7, Ni_5Zr, $Ni_{23}Zr_6$, Ni_7Zr_2, Ni_3Zr, $Ni_{21}Zr_8$, $Ni_{10}Zr_7$, NiZr and $NiZr_2$ intermetallic compounds are stable phases [32,42]. Besides, the calculated heats of formation for Ni_2Zr and $Ni_{11}Zr_9$ phases are −43.616 and −41.466 kJ/mol atoms, and they lie about 5.869 and 8.019 kJ/mol atoms above the ground state convex hull, respectively. These results indicate that the Ni_2Zr and $Ni_{11}Zr_9$ intermetallic compounds are metastable phases, which can further be decomposed into other stable phases, i.e. $Ni_2Zr \rightarrow Ni_{10}Zr_7 + Ni_{21}Zr_8$ and $Ni_{11}Zr_9 \rightarrow NiZr + Ni_{10}Zr_7$ [11,22,43]. Moreover, the calculated heats of formation for these binary Ni–Zr intermetallic compounds are all negative, i.e. −37.108, −40.465, −46.863, −49.485, −47.655, −43.616, −48.216, −41.466, −48.137 and −33.817 kJ/mol atoms for Ni_5Zr, $Ni_{23}Zr_6$, Ni_7Zr_2, Ni_3Zr, $Ni_{21}Zr_8$, Ni_2Zr, $Ni_{10}Zr_7$, $Ni_{11}Zr_9$, NiZr and $NiZr_2$, respectively. These large negative values suggest that the chemical interaction between Ni and Zr is very strong [8,10,26,28,34], and also imply that these binary Ni–Zr intermetallic compounds are thermodynamically stable.

3.3.2. Cohesive energy

The cohesive energy which is considered as another thermodynamic parameter to measure the structural stability of materials, defines to be the required energy for separating the metallic crystals into the individual neutral free atoms at infinite separation; i.e. it is the difference between the total energy of isolated atom and the total energy of crystals [75–77]. With this definition, the cohesive energy is a positive number. For a given binary Ni_aZr_b intermetallic compound, its cohesive energy can be obtained via the following formula (7):

$$E_{\text{coh}}^{\text{Ni}_a\text{Zr}_b} = \left(aE_{\text{atom}}^{\text{Ni}} + bE_{\text{atom}}^{\text{Zr}} - E_{\text{cryst}}^{\text{Ni}_a\text{Zr}_b}\right)/(a+b) \tag{7}$$

Concretely, in formula (7), $E_{\text{coh}}^{\text{Ni}_a\text{Zr}_b}$ denotes the cohesive energy of Ni_aZr_b crystalline phase, $E_{\text{cryst}}^{\text{Ni}_a\text{Zr}_b}$ is the total energy of the Ni_aZr_b

Table 5
The cohesive energy for the binary Ni–Zr system intermetallic compounds, calculated in this work and known from the literature.

Phase	Cohesive energy (eV/atom)	Reference
Ni	5.202	This work
	4.450	[27]
	5.600	[30]
Ni_5Zr	5.898	This work
$Ni_{23}Zr_6$	6.008	This work
Ni_7Zr_2	6.104	This work
Ni_3Zr	6.182	This work
	5.357	[27]
	5.345	[27]
$Ni_{21}Zr_8$	6.212	This work
Ni_2Zr	6.276	This work
Aba2-$Ni_{10}Zr_7$	6.470	This work
Pbca-$Ni_{10}Zr_7$	6.470	This work
$Ni_{11}Zr_9$	6.471	This work
NiZr	6.633	This work
$NiZr_2$	6.794	This work
Zr	7.062	This work
	6.250	[27]
	6.256	[30]

primitive cell containing "*a*" Ni atoms and "*b*" Zr atoms with its stable ground state structure, E_{atom}^{Ni} is the energy of one Ni atom and E_{atom}^{Zr} is the energy of one Zr atom. Accordingly, the energy of these binary Ni–Zr intermetallic compounds and the isolated Ni atom as well as Zr atom has been calculated to obtain their respective cohesive energies. The results are summarized in Table 5, along with the available values known from the literatures [27,30]. Correspondingly, the cohesive energies versus Zr-content for these Ni–Zr intermetallic compounds are further depicted in Fig. 8. As we can see that the cohesive energy of these binary Ni–Zr intermetallic compounds increases with the increase of Zr-content, thus signifying that the structural stability of these binary Ni–Zr intermetallic compounds increases with Zr-content increasing. We also note that the strength of the chemical interactions between Ni and Zr increases with Zr-content increasing, given that the cohesive energy can be used to reflect the structural stability and the strength of metallic interactions between different componential elements [39,77–79].

In addition, the large value of cohesive energy for these binary Ni–Zr intermetallic compounds also implies the strong chemical interactions between Ni and Zr elements. This is consistent with previous studies which indicated that the transition metals Ni and Zr are characterized by high binding energy [10,27,34,37].

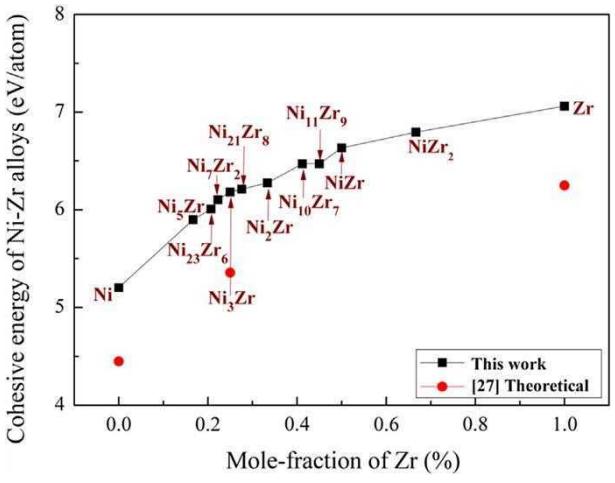

Fig. 8. Calculated cohesive energy compared to other theoretical values known from the literature for the binary Ni–Zr intermetallic compounds.

3.4. The electronic properties

Based on their respective optimized structures, the electronic energy band structures and corresponding density of states (DOS) for these binary Ni–Zr intermetallic compounds have been obtained by performing first-principles calculations. The results are depicted in Figs. 9 and 10, where the dot dash line zero-point energy signifies the Fermi energy level (E_F) defined to be the highest energy level occupied by the valence electrons at 0 K. The electronic energy band structures of these binary Ni–Zr intermetallic compounds represent the energy of points along with high symmetry directions. As the electronic energy band structures and corresponding total density of states (TDOS) reflected in Fig. 9, the valence band overlaps with the conduction band at the Fermi surface for Ni_5Zr, $Ni_{23}Zr_6$, Ni_3Zr, $Ni_{21}Zr_8$, Ni_2Zr, Aba2-$Ni_{10}Zr_7$, Pbca-$Ni_{10}Zr_7$, $Ni_{11}Zr_9$, Ni_7Zr_2, NiZr and $NiZr_2$. This indicated that these binary Ni–Zr intermetallic compounds exhibit the metallic conductivity. Meanwhile, the density of states corresponding to the Fermi surface was not zero, which also implies that all of these binary Ni–Zr intermetallic compounds are conductive phases. According to the partial density of states, we can see that the major valence electron contributions to the bonding electrons in the whole regions are dominated by Ni (3d) and Zr (4d). The band positions of Ni (3d) almost unchanged in the whole regions, while both the band positions and shapes of Zr (4d) changed distinctly for these binary Ni–Zr intermetallic compounds. Below the Fermi surface, the Ni-d states and Zr-d states show evidence for hybridization in the valence band of these binary Ni–Zr intermetallic compounds. The Ni–Zr bonding states are occupied with the center of the band located at about 2 eV below the Fermi surface. The regions above the Fermi surface are the conduction band, which are mainly contributed by the Zr-d electrons for these binary Ni–Zr intermetallic compounds; as the DOS reflected in Fig. 10.

In addition, it can be deduced that the bonding electron numbers per atom below the Fermi surface are 10.31, 10.40, 10.43, 10.50, 10.54, 10.65, 10.81, 10.89, 10.99 and 11.32 for Ni_5Zr, $Ni_{23}Zr_6$, Ni_7Zr_2, Ni_3Zr, $Ni_{21}Zr_8$, Ni_2Zr, $Ni_{10}Zr_7$, $Ni_{11}Zr_9$, NiZr and $NiZr_2$, respectively. The larger number of bonding electrons usually implies the stronger interactions between the charges and the better structural stability of an alloy phase [80–82]. Thus it also reflects the variation trend of the structural stability versus Zr-content for these binary Ni–Zr intermetallic compounds, which agree completely with discussions in the previous section. Moreover, with the distance increasing from the nearest peaks to the zero energy symbolized bands, the bonds transformed from metallic to covalent [69,83]. These peaks are close to each other for these binary Ni–Zr intermetallic compounds, which also demonstrate their metallicity. In general, the ductility of an alloy phase may decrease as the metallicity of bond becoming weaker. As the DOS shown in Fig. 10, the corresponding distance of $NiZr_2$ is the minimum among these binary Ni–Zr alloy phases, implying that it possesses the strongest metallicity and hence it has the best ductility among these binary Ni–Zr intermetallic compounds. This result is in accordance with the ductility estimated from the G/K and Poisson's ratio values. Besides, the density of states at Fermi energy level N(E_F) for these binary Ni–Zr intermetallic compounds is mainly dominated by Ni-d and Zr-d electrons. Furthermore, the structural stability of intermetallic compounds can be judged from the position of Fermi surface in the density of states curve [84,85]. As can be seen in Fig. 10, the E_F falls exactly on the pseudogap (deep valley

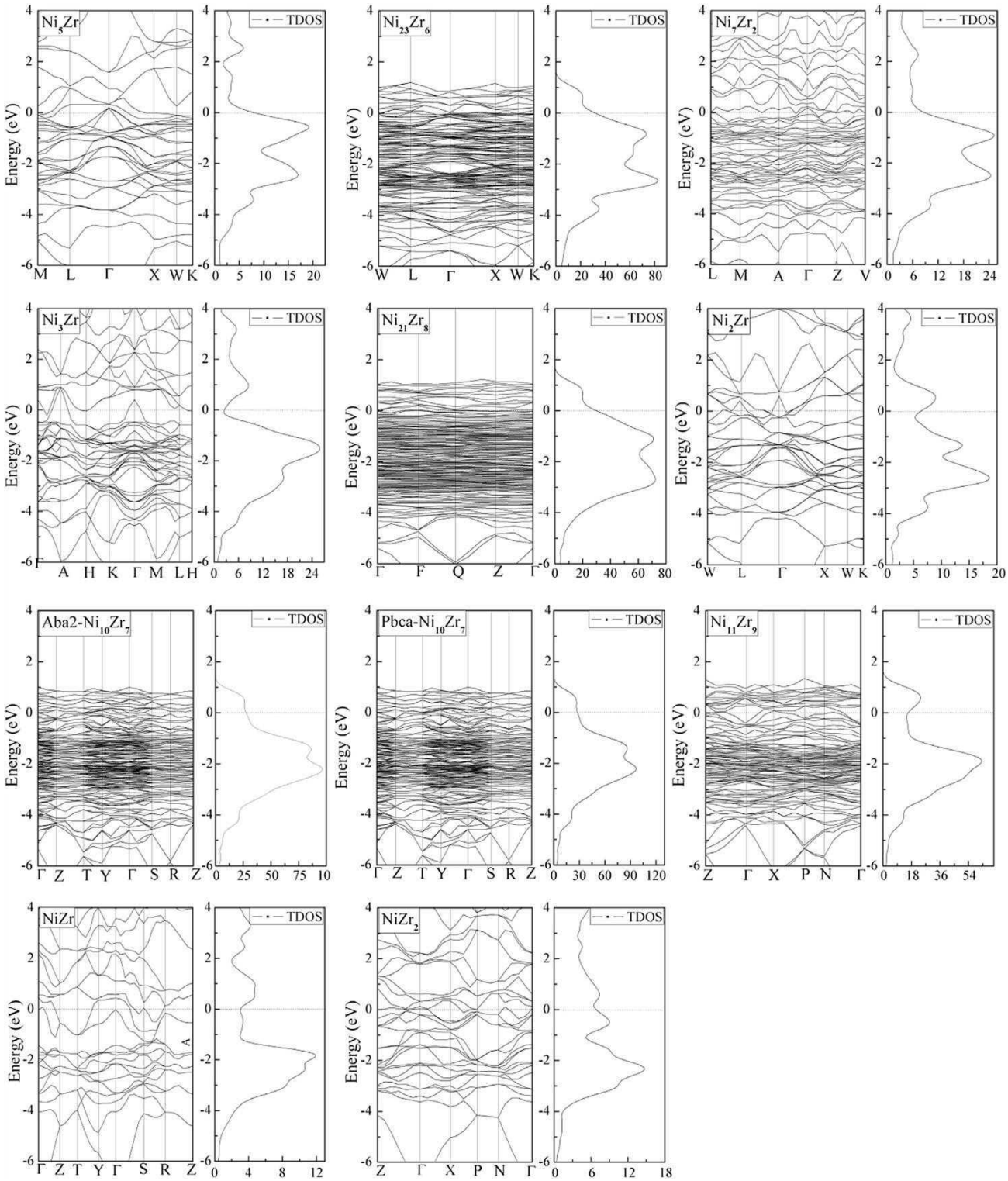

Fig. 9. Calculated electronic energy band structures and the corresponding total density of states (TDOS) for the binary Ni–Zr system intermetallic compounds.

close to E_F) for Ni_3Zr and NiZr intermetallic compounds, and their N(E_F) value is low (0.31 and 0.75 states/eV/atom for Ni_3Zr and NiZr, respectively), thus implying their structural stability and also their high melting points. The E_F lies to the left of the pesudogap (i.e. within the bonding states) for $NiZr_2$, $Ni_{10}Zr_7$, $Ni_{21}Zr_8$, Ni_5Zr, $Ni_{23}Zr_6$ and Ni_7Zr_2 intermetallic compounds, and their corresponding N(E_F) values are low, suggesting they are structurally stable alloy phases. While for Ni_2Zr and $Ni_{11}Zr_9$ intermetallic compounds, the E_F lies to the right of the pesudogap (i.e. within the antibonding states) in the DOS curve and their N(E_F) are relatively high (1.05 and 0.80 states/eV/atom for Ni_2Zr and $Ni_{11}Zr_9$), which indicated that they are the metastable phases and will decompose into other stable phases. So in line with the results obtained from the heats of formation and in line with the experimental investigations [11,22,43].

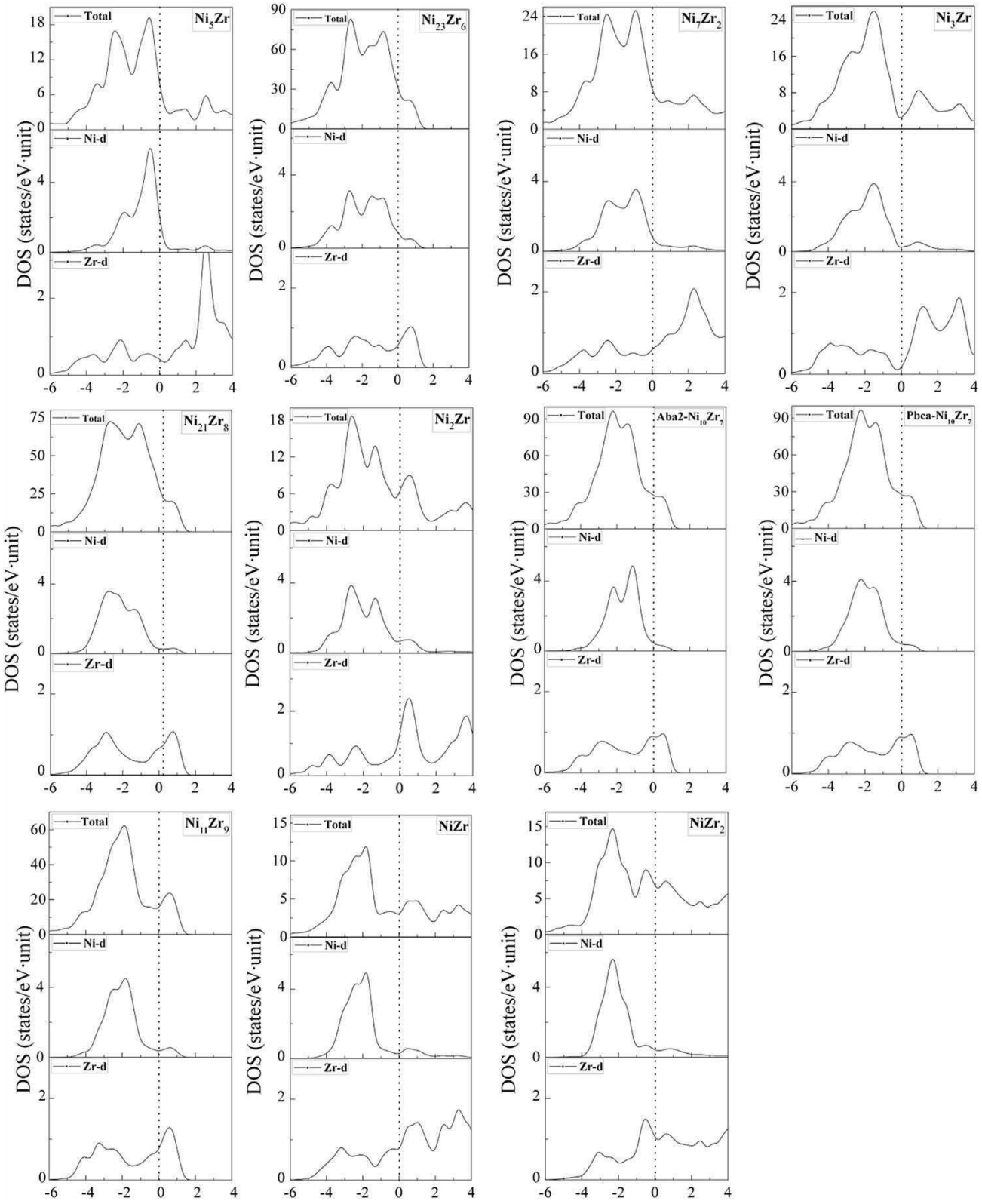

Fig. 10. Calculated density of states (DOS) for the binary Ni–Zr system intermetallic compounds.

4. Conclusion

In conclusion, first-principles calculations have been performed to investigate the structural, mechanical, thermodynamic and electronic properties of the binary Ni–Zr intermetallic compounds. The results indicated that the lattice parameters after optimization are in good agreement with the available experimental and other theoretical values. Besides, the mass density and bulk modulus of

these binary Ni–Zr intermetallic compounds decrease with Zr-content increasing. The intermetallic compounds Ni_5Zr, $Ni_{23}Zr_6$, Ni_7Zr_2, Ni_3Zr, Ni_2Zr, Aba2-$Ni_{10}Zr_7$, Pbca-$Ni_{10}Zr_7$, $Ni_{11}Zr_9$, NiZr and $NiZr_2$ are mechanically stable phases.

Furthermore, the polycrystalline elastic moduli of these binary Ni–Zr intermetallic compounds were obtained from their respective single-crystal elastic constants via VRH approximations. Among these Ni–Zr intermetallic compounds, the Ni_5Zr phase possesses the largest elastic modulus and hence has the largest stiffness and the highest hardness; while the $NiZr_2$ is the most ductile phase. The investigation of thermodynamic and electronic properties indicated that the structural stability of these binary Ni–Zr intermetallic compounds increases with Zr-content increasing, and these binary Ni–Zr alloy phases are thermodynamically stable. Furthermore, results on the electronic properties demonstrated that all the binary Ni–Zr intermetallic compounds considered here are conductive phases.

Acknowledgments

This work was supported by the National Natural Science Foundation of China (Grant nos. 51121061, 51131002 and 51372215), the Key Basic Research Program of Hebei Province of China (Grant no. 12965135D) and the Natural Science Foundation for Distinguished Young Scholars of Hebei Province of China (Grant no. E2013203265). R. M. acknowledges the support from the NSERC and CRC programs, Canada. The authors also would like to thank the staff of the Center for Computational Materials Science, Institute for Materials Research, Tohoku University for computer support. Y. K. is thankful to the CREST project headed by Prof. M. Kotani.

References

[1] Huang L, Li S. J Mater 2013;2013:575640.
[2] Metikos-Hukovic M, Jukic A. Electrochim Acta 2000;45:4159.
[3] Ismail N, El-Meligi AA, Uhlemann M, Gebert A, Eckert J, Schultz L. J Alloys Compd 2009;480:321.
[4] Jukic A, Piljac J, Metikos-Hukovic M. J Mol Catal A 2001;166:293.
[5] Nagase T, Takizawa K, Umakoshi Y. Intermetallics 2011;19:511.
[6] Inoue A, Nishiyama N. MRS Bull 2007;32:651.
[7] Liu YH, Wang G, Wang RJ, Zhao DQ, Pang MX, Wang WH. Science 2007;315:1385.
[8] Kokanovic I, Tonejc A. Mater Sci Eng A 2004;373:26.
[9] Miedema AR, De Boer FR, Boom R. Phys B 1981;103:67.
[10] Basu J, Murty BS, Ranganathan S. J Alloys Compd 2008;465:163.
[11] Abe T, Onodera H, Shimono M, Ode M. Mater Trans 2005;46:2838.
[12] Altounian Z, Guohua Tu, Stromolsen JO. J Appl Phys 1983;54:3111.
[13] Altounian Z, Stromolsen JO. Phys Rev B 1983;27:4149.
[14] Bormann R, Gartner F, Zoltzer K. J Less-Common Met 1988;145:19.
[15] Weeber AW, Bakker H. J Phys F 1988;18:1359.
[16] Li S, Xie GQ, Louzguine-Luzgin DV, Inoue A. Mater Trans 2008;49:494.
[17] Mckamey CG, Kroeger DM, Easton DS, Scarbrough JO. J Mater Sci 1986;21:3863.
[18] Easton DS, Mckamey CG, Kroeger DM, Cavin OB. J Mater Sci 1986;21:1275.
[19] Eckert J, Schultz L, Hellstern E, Urban K. J Appl Phys 1988;64:3224.
[20] Lee PY, Koch CC. Appl Phys Lett 1987;50:1578.
[21] Lee PY, Koch CC. J Mater Sci 1988;23:2837.
[22] Gavrichev KS, Golushina LN, Gorbunov VE, Zaitsev AI, Zaitseva NE, Mogutnov BM, et al. J Phys Condens Matter 2004;16:1995.
[23] Sprianoa S, Rosalbino F, Baricco M, Morra PV, Angelini E, Antonione C, et al. Intermetallics 2000;8:299.
[24] Flege S, Hahn H, Averback R. Phys Rev B 2004;69:014303.
[25] Wang YM, Shek CH, Qiang JB, Wong CH, Wang Q, Zhang XF, et al. Mater Trans 2004;45:1180.
[26] Liu XJ, Hui XD, Chen GL, Liu T. Phys Lett A 2009;373:2488.
[27] Dai Y, Li JH, Liu BX. J Appl Phys 2012;111:033521.
[28] Li YH, Zhang W, Dong C, Qiang JB, Makino A, Inoue A. Intermetallics 2010;18:1851.
[29] Lee A, Etherington G, Wagner CNJ. J Non-Cryst Solids 1984;61:349.
[30] Bozzolo G, Mosca HO, del Grosso MF. Intermetallics 2008;16:668.
[31] Ma D, Tan H, Wang D, Li Y, Ma E. Appl Phys Lett 2005;86:191906.
[32] Henaff MP, Colinet C, Pasturel A, Buschow KHJ. J Appl Phys 1984;56:307.
[33] Altounian Z, StromOlsen JO, Walter JL. J Appl Phys 1984;55:1566.
[34] Clemens BM, Gllgenbach RM, Bidwell S. Appl Phys Lett 1987;50:495.
[35] Barbour JC, de Reus R, Denier van der Gon AW, Saris FW. J Mater Res 1987;2:168.
[36] Frahm R, Haensel R, Rabe P. J Phys Condens Matter 1989;1:1521.
[37] Wong GC, Johnson WL, Cotts EJ. J Mater Res 1990;5:488.
[38] Ohsaka K, Trinh EH, Holzer JC, Johnson WL. Appl Phys Lett 1993;62:2319.
[39] Jaksic MM, Lacnjevac CM, Grgurc BN, Krstajic NV. J Mat Electr Sys 2000;3:131.
[40] Joubert JM, Latroche M, Percheron-Guegan A. J Alloys Compd 1995;231:494.
[41] Mihailov L, Spassov T, Bojinov M. Int J Hydrogen Energy 2012;37:10499.
[42] Nash P. Phase diagrams of the binary nickel system. Metals Park, OH: ASM International; 1991 [Review].
[43] Gupta KP. J Phase Equil 2000;21:485.
[44] Villars P, Calvert LD. Pearson's handbook of crystallographic data for intermetallic phases. Materials Park (OH): ASM International; 1997.
[45] Kresse G, Marsman M, Furthüller J. VASP the guide http://cms.mpi.Univie.ac.at/vasp/.
[46] Payne MC, Teter MP, Allan DC, Arias TA, Joannopoulous JD. Rev Mod Phys 1992;64:1045.
[47] Blöchl PE. Phys Rev B 1994;50:17953.
[48] Monkhorst HJ, Pack JD. Phys Rev B 1976;13:5188.
[49] Wen B, Shao TJ, Melnik R, Kawazoe Y, Tian YJ. J Appl Phys 2013;113:103501.
[50] Shao TJ, Wen B, Melnik R, Yao S, Kawazoe Y. J Appl Phys 2012;111:083525.
[51] Zhao JJ, Winey JM, Gupta YM. Phys Rev B 2007;75:094105.
[52] Catti BM. Acta Crystallogr Sect A 1985;41:494.
[53] Thakur KP. J Phys F Met Phys 1985;15:2421.
[54] Epstein SG, Carlson ON. Acta Metal 1965;13:487.
[55] Fast Lars, Wills JM, Johansson Borje, Eriksson O. Phys Rev B 1995;51:17431.
[56] Ghosh G. Acta Mater 2007;55:3347.
[57] Yuan XL, Xue MA, Chen W, An TQ, Cheng Y. Comp Mater Sci 2012;65:127.
[58] Wu ZJ, Zhao EJ, Xiang HP, Hao XF, Liu XJ, Meng J. Phys Rev B 2007;76:054115.
[59] Anderson OL. J Phys Chem Solids 1963;24:909.
[60] Chung DH, Buessem WR. J Appl Phys 1968;39:2777.
[61] Kane RH, Giessen BC, Grant NJ. Acta Met 1966;14:605.
[62] Pauly S. Acta Mater 2009;57:5445.
[63] Music D, Schneider JM. Appl Phys Lett 2006;89:121914.
[64] Haines J, Leger JM, Bocquillon G. Annu Rev Mater Res 2001;31:1.
[65] Sahara R, Shishido T, Nomura A, Kudou K, Okada S, Kumar V, et al. Phys Rev B 2007;76:0241051.
[66] Pugh SF. Philos Mag 1954;45:823.
[67] Ganeshan S, Shang SL, Zhang H, Wang Y, Mantina M, Liu ZK. Intermetallics 2009;17:313.
[68] Sangiovanni DG, Chirita V, Hultman L. Phys Rev B 2010;81:104107.
[69] Zhou Y, Wen B, Ma YQ, Melnik R, Liu XJ. J Solid State Chem 2012;187:211.
[70] Du JL, Wen B, Melnik R, Kawazoe Y. J Alloys Compd 2014;588:96.
[71] Gschneidner Jr K, Russell A, Pecharsky A, Morris J, Zhang Z, Lograsso T, et al. Nat Mater 2003;2:587.
[72] Greaves GN, Greer AL, Lakes RS, Rouxel T. Nat Mater 2011;10:823.
[73] Cui SX, Xiao XG, Hu HQ, Lv ZT, Zhang GQ, Gong ZZ. Phys B 2011;406:3389.
[74] Kunzi HU. Top Appl Phys 1983;53:169.
[75] Qi WH, Wang MP, Xu GY. Chem Phys Lett 2003;372:632.
[76] Perger WF, Pandey Ravindra, Blanco Miguel A, Zhao JJ. Chem Phys Lett 2004;388:175.
[77] Razumovskiy Vsevolod I, Ruban AV, Razumovskii IM, Lozovoi AY, Butrim VN, Vekilov Yu Kh. Scr Mater 2011;65:926.
[78] Ahmed R, Hashemifar SJ, Akbarzadeh H. Phys B 2007;400:297.
[79] Kittel C, McEuen P. Introduction to solid state physics. New York: Wiley; 1996.
[80] Fu CL, Wang XD, Ye YY, Ho KM. Intermetallics 1999;7:179.
[81] Tao XM, Jund P, Colinet C, Tedenac JC. Phys Rev B 2009;80:104103.
[82] Wang XB, Tian DC, Wang LL. J Phys Condens Matter 1994;6:10185.
[83] Hoffmann R. Rev Mod Phys 1988;60:601.
[84] Ravindran P, Asokamani R. Bull Mater Sci 1997;20:613.
[85] Hong T, Yang TJW, Guo XQ, Freeman AJ, Oguchi T, Xu JH. Phys Rev B 1991;43:1940.